nature photonics

LETTERS

PUBLISHED ONLINE: 12 OCTOBER 2014 | DOI: 10.1038/NPHOTON.2014.228

Probing the mechanisms of large Purcell enhancement in plasmonic nanoantennas

Gleb M. Akselrod[1,2], Christos Argyropoulos[1,2], Thang B. Hoang[1,3], Cristian Ciracì[1,2†], Chao Fang[2], Jiani Huang[1,3], David R. Smith[1,2,3] and Maiken H. Mikkelsen[1,2,3*]

To move nanophotonic devices such as lasers and single-photon sources into the practical realm, a challenging list of requirements must be met, including directional emission[1–5], room-temperature and broadband operation[6–9], high radiative quantum efficiency[1,4] and a large spontaneous emission rate[7]. To achieve these features simultaneously, a platform is needed for which the various decay channels of embedded emitters can be fully understood and controlled. Here, we show that all these device requirements can be satisfied by a film-coupled metal nanocube system with emitters embedded in the dielectric gap region. Fluorescence lifetime measurements on ensembles of emitters reveal spontaneous emission rate enhancements exceeding 1,000 while maintaining high quantum efficiency (>0.5) and directional emission (84% collection efficiency). Using angle-resolved fluorescence measurements, we independently determine the orientations of emission dipoles in the nanoscale gap. Incorporating this information with the three-dimensional spatial distribution of dipoles into full-wave simulations predicts time-resolved emission in excellent agreement with experiments.

Typical luminescent emitters have relatively long emission lifetimes (~10 ns) and non-directional emission. Unfortunately, these intrinsic optical properties are poorly matched to the requirements of nanophotonic devices. For example, in single-photon sources, fast radiative rates are required for operation at high frequencies, and directionality is needed to achieve a high collection efficiency[10]. In addition, with plasmonic lasers, enhanced spontaneous emission into the cavity mode can reduce the lasing threshold[9]. As a result, much work has focused on modifying the photonic environment of emitters to enhance[11] the spontaneous emission rate, known as the Purcell effect[12]. Early approaches concentrated on integrating emitters into dielectric optical microcavities and showed modest emission rate enhancements[13–15]. However, dielectric cavities require high quality factors for large rate enhancements, which makes these cavities mismatched with the spectrally wide emission from inhomogeneously broadened or room-temperature emitters. Plasmonic nanostructures are a natural solution to the spectral mismatch problem because of their relatively broad optical resonances and high field enhancements[16–18]. Despite these advantages and the capability for emission rate enhancement[19], many plasmonic structures suffer from unacceptably high non-radiative decay due to intrinsic losses in the metal, or have low directionality of emission[7]. In plasmonic structures, the Purcell factor (defined as the fractional increase in total emission rate) has contributions from an increased radiative rate and from an increased non-radiative rate due to metal losses. It is therefore critical to specify the fraction of energy emitted as radiation, known as the radiative quantum efficiency (QE). From knowledge of the Purcell factor and the QE, the enhancement in the radiative rate can be obtained.

The largest field enhancements occur in nanoscale gaps between metals, but these are challenging to fabricate reliably, especially on a large scale. Plasmonic antenna designs such as bowtie antennas rely on gaps defined laterally using electron-beam lithography[20] or ion milling[21], making it difficult to produce the sub-10-nm gaps for which the highest Purcell factors occur. A promising geometry that overcomes these challenges is the plasmonic patch antenna, which consists of emitters situated in a vertical gap between a metal disk and a metal plane[22–24]. Because this enables a planar fabrication technique, the gaps in patch antennas can be controlled with nanometre[25] and sub-nanometre[26] precision. To date, however, micrometre-scale plasmonic patch antennas have shown only modest emission rate enhancements (~80) and low radiative QE[23,27].

In this Letter we demonstrate a nanoscale patch antenna (NPA) that has large emission rate enhancement, high radiative efficiency, directionality of emission, and deep sub-wavelength dimensions. The NPA consists of a colloidally synthesized silver nanocube (side length of ~80 nm) situated over a metal film, separated by a well-controlled nanoscale gap (5–15 nm) embedded with emitters (Fig. 1a,b). The fundamental plasmonic mode of the film-coupled nanocube is localized in the gap (Fig. 1c) with the dominant electric field oriented in the vertical (z) direction, transverse to the gap. The resonance wavelength is determined by the size of the optical resonator, defined by the side length of the nanocube and the thickness and refractive index of the gap material[25]. The resonance of such NPAs can be tuned from 500 nm to 900 nm by controlling these dimensions[25,28]. On resonance, the maximum field enhancements in the gap can reach 200 (ref. 29), resulting in up to 30,000-fold fluorescence intensity enhancement of molecules integrated into the gap[29], as well as enhanced Raman scattering[24].

Through full-wave simulations, the radiation pattern of the antenna at the resonance wavelength is predicted to have a single lobe oriented in the surface-normal direction (Fig. 1d). The fraction of emitted light collected by the first lens[1] is calculated to be 84% using an objective lens with a numerical aperture of NA = 0.9. The scattered radiation pattern of a single NPA was measured by imaging the back of the objective lens, and showed excellent agreement with simulations (Fig. 1d). Emission at angles greater than 64° falls outside the collection cone of the NA = 0.9 objective lens, explaining the small discrepancy between measurements and simulations. Although the NPA is less directional than multi-element plasmonic antennas such as the Yagi–Uda antenna[2], the main radiation lobe of the NPA is normal to the surface, an important

[1]Center for Metamaterials and Integrated Plasmonics, Duke University, Durham, North Carolina 27708, USA, [2]Department of Electrical and Computer Engineering, Duke University, Durham, North Carolina 27708, USA, [3]Department of Physics, Duke University, Durham, North Carolina 27708, USA; [†]Present address: Istituto Italiano di Tecnologia (IIT), Center for Biomolecular Nanotechnologies, Via Barsanti, I-73010 Arnesano, Italy.
*e-mail: m.mikkelsen@duke.edu

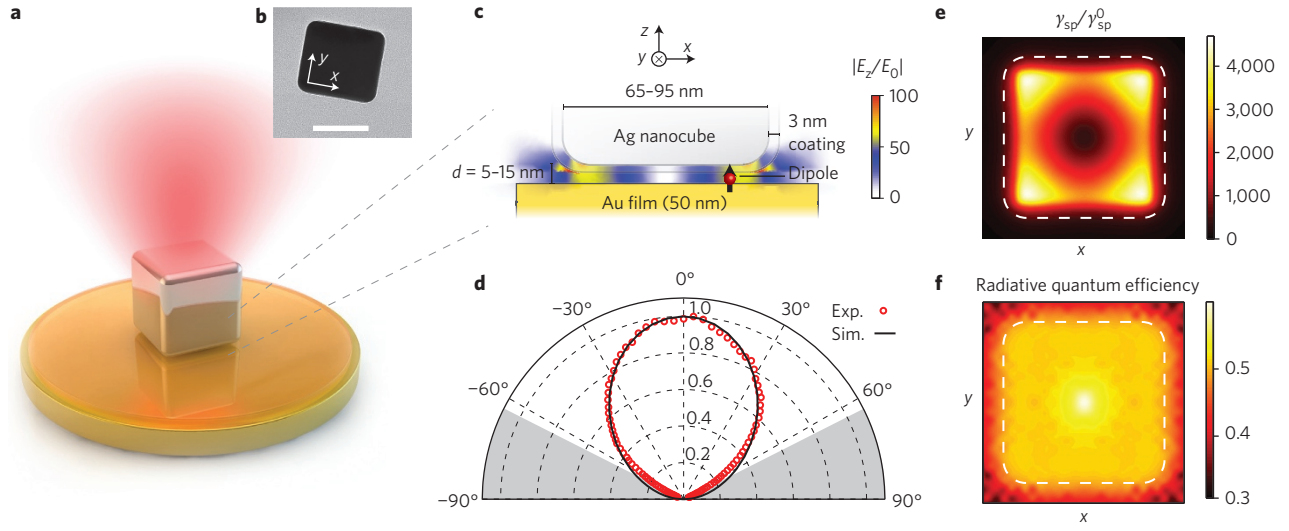

Figure 1 | Directional plasmonic nanopatch antenna. a, Schematic of a silver nanocube situated on a gold film separated by a 5–15 nm spacer layer containing a fluorescent material. The red cone indicates the directionality of the enhanced emission originating from the nanogap region. **b**, Transmission electron microscopy image of a single silver nanocube. Scale bar, 50 nm. **c**, Schematic cross-section of a film-coupled silver nanocube showing the simulated fundamental plasmonic gap mode with maximum field enhancement of ~100. The dominant component of the gap electric field is in the vertical (z) direction and is largest near the corners of the nanocube. **d**, Simulated (black) and measured (red) radiation pattern from a single nanoscale patch antenna, showing that most emission (84%) falls within the numerical aperture of the objective lens (NA = 0.9). Grey regions represent angular regions that were not collected. **e**,**f**, Maps of enhancement of the spontaneous emission rate and of the quantum efficiency relative to a dipole in free space as a function of position under the nanocube. The white dashed line indicates the lateral extent of the nanocube. In this simulation, dipoles are assumed to be vertically oriented for maximum coupling to the gap mode and have a free-space quantum efficiency of $QE_0 = 0.2$.

feature for applications such as single-photon sources where coupling to external optics is needed.

Due to the large field enhancement and increased density of states, emitters placed in the nanogap experience large changes in their spontaneous emission rate. In general, the spontaneous emission rate of a dipole is given by

$$\gamma_{sp}(\mathbf{r}) = \frac{\pi\omega}{3\hbar\,\epsilon_0}|\mathbf{p}|^2\rho(\mathbf{r},\omega) + \gamma^0_{int} \quad (1)$$

where ω is the emission frequency, $\mathbf{p}$ is the transition dipole moment of the emitter, $\mathbf{r}$ is the position, ϵ_0 is the permittivity of free space and γ^0_{int} is the internal non-radiative decay rate of the emitter. In the plasmonic environment, the large field greatly enhances the local density of states:

$$\rho(\mathbf{r},\omega) \propto \hat{\mathbf{n}}_p \cdot \mathrm{Im}\{G(\mathbf{r},\mathbf{r})\} \cdot \hat{\mathbf{n}}_p \quad (2)$$

where $\hat{\mathbf{n}}_p$ is the orientation of the transition dipole of the emitter and G is the dyadic Green's function, which is the electric field interacting with the emitter due to its own radiation. Figure 1e,f presents maps of the emission properties of an NPA with a plasmon resonance of $\lambda_{np} = 650$ nm and a gap thickness of $d = 8$ nm computed by full-wave simulations (see Methods). When the emitters are resonant with the plasmon mode, the NPA shows dramatic enhancement in the spontaneous emission rate γ_{sp} relative to the emission rate in free space, γ^0_{sp} (Fig. 1e). The calculated emission rate depends on the lateral position of the emitter under the nanocube, with rate enhancements exceeding 4,000 near the corners of the nanocube for dipoles oriented along the z direction. At the same time, the emission efficiency remains high (>0.5) and spatially uniform (Fig. 1f), quantified by the radiative quantum efficiency $QE = \gamma_r/\gamma_{sp}$, where γ_r is the radiative rate of the emitter.

Observing large emission rate enhancements experimentally is often challenging due to the intrinsic lifetime of many common emitters (~10 ns) and the temporal resolution limit of single-photon detectors (~30 ps). To overcome this limitation, we used a fluorescent ruthenium metal complex dye (Ru dye) with a long intrinsic lifetime of $\tau_0 = 1/\gamma^0_{sp} = 600 \pm 50$ ns (Fig. 2a,e). The nanogap of the NPA was fabricated by growing a layer-by-layer polyelectrolyte film with controlled thickness (2–12 nm) on a gold film (Fig. 2b). The samples were immersed in a solution of Ru dye, allowing the dye to intercalate into the polymer film. This was followed by immersing the sample in a solution containing silver nanocubes covered in a 3-nm-thick polymer coating, which electrostatically adhered to the polymer film, completing the structure (see Methods). Individual antennas were identified by dark-field microscopy and spectroscopy (see Methods), and those with a plasmon resonance of $\lambda_{np} = 620$–650 nm were selected for good spectral overlap with the Ru dye emission (Fig. 2a). The large wavelength shift between absorption and emission of the Ru dye allowed for non-resonant excitation at $\lambda_{ex} = 535$ nm (Fig. 2a). The relationship between nanocube size, gap size and plasmon resonance has been established previously[25].

Figure 2e shows the time-resolved emission from a single NPA with a $d = 8$ nm gap after non-resonant pulsed excitation at $\lambda_{ex} = 535$ nm (see Methods). The emission shows a non-exponential decay with an initial rate at $t = 0$ of $\gamma^{max}_{sp} = 1/0.7\ \mathrm{ns}^{-1}$, corresponding to a maximum spontaneous emission rate enhancement, also called the Purcell enhancement, of $\gamma^{max}_{sp}/\gamma^0_{sp} = 860$. The slower decay rates contributing to the emission result from the spatial dependence of the rate enhancement (Fig. 1e). Similar results were obtained for nine other NPAs. The distribution of emission rate constants was extracted by fitting the time-resolved fluorescence to a stretched exponential and then decomposing the fit function into a sum of rate constants by performing a Laplace transform (Supplementary Figs 2 and 3). The extracted distribution shows that a fraction of Ru molecules is optimally positioned, with $\gamma^{max}_{sp}/\gamma^0_{sp}$ approaching 1,000, while the most likely enhancement from the NPA is $\gamma^*_{sp}/\gamma^0_{sp} = 60$ (Fig. 2e). We note that other fit functions for the time-resolved fluorescence produced slightly different rate distributions (Supplementary Fig. 4). However, the choice of

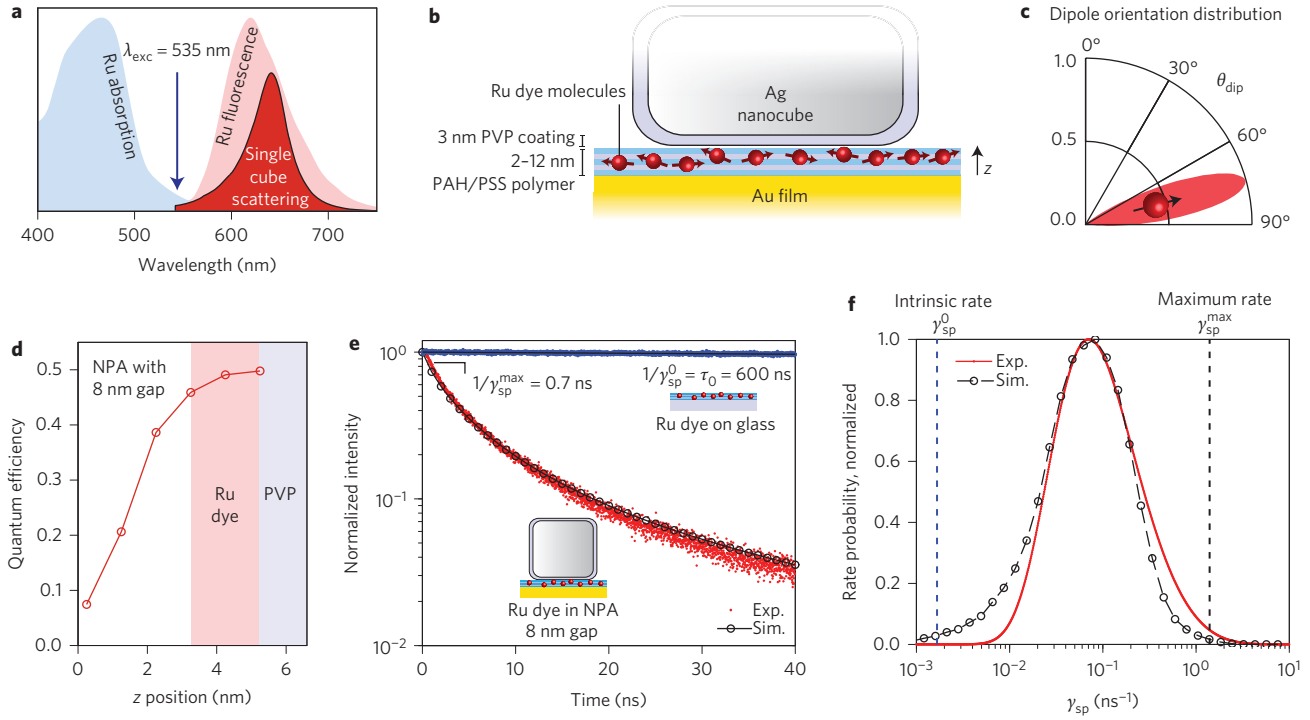

Figure 2 | Experimental demonstration of large spontaneous emission rate enhancement. a, Absorption and fluorescence spectrum of the Ru dye. The dye fluorescence spectrum overlaps with the film-cube resonance at $\lambda_{np} \approx 650$ nm. The nanoscale patch antennas (NPAs) were excited non-resonantly at $\lambda_{ex} \approx 535$ nm. **b**, Cross-section of the experimental structure consisting of Ru dye intercalated into a polymer film and situated between a gold film and a silver nanocube. Arrows indicate typical directions of the transition dipole moments. **c**, Angular distribution of Ru-dye transition dipole moments in the polymer film as determined from angle- and polarization-resolved fluorescence measurements. Most dipoles were found to be nearly parallel to the gold surface, $\theta_{dip} = 75°$, where 0° corresponds to the surface normal. **d**, Simulated quantum efficiency for emitters at varying distances from the gold film in the NPA with an 8 nm gap. **e**, Comparison of the measured time-resolved fluorescence decay for Ru dye on glass and Ru dye enhanced by a single nanoantenna with a $d = 8$ nm gap. The intrinsic lifetime of the Ru dye on glass is $1/\gamma_{sp}^{0}$. In the nanoantenna, a fast non-exponential decay in fluorescence is observed, with a minimum lifetime of $1/\gamma_{sp}^{max} = 0.7$ ns. **f**, Experimental and simulated distribution of Ru-dye emission rates $H(\gamma_{sp})$ from the NPA. The experimental distribution is obtained from a fit of the time-resolved fluorescence to a stretched exponential.

function does not affect the maximum rate enhancement, which is obtained from the slope of the fluorescence decay at $t = 0$.

A critical parameter in correctly simulating the optical response of the NPA is the orientation of the emitter transition dipoles relative to the gap mode electric field. However, in many plasmon-enhanced fluorescence studies, the dipole orientation distribution is assumed to be isotropic[23,30] or to have an optimal orientation[31]. Here, we directly determine the distribution of dipole orientations by angle- and polarization-resolved fluorescence measurements of Ru dye embedded in a polymer film (see Supplementary Information and Supplementary Figs 8–12). The measurements reveal that most emission dipoles are oriented at 75° relative to the surface normal (Fig. 2c). Although this orientation reduces the maximum rate enhancements observed, this feature is specific to the Ru dye in these polymer films and, in general, the emitter orientation can be engineered through chemical means[32]. Furthermore, the simulations show that the QE depends on the vertical position of the emitters in the gap, with emitters close to the gold surface experiencing increased non-radiative quenching (Fig. 2d).

The simulated temporal decay curves were obtained by assuming that dipoles are distributed uniformly in the plane of the gap and in the top 2 nm of the spacer polymer film. The emission from a dipole at position $\mathbf{r}$ and angle θ is given by

$$I(\mathbf{r},\theta,t) \propto \gamma_r(\mathbf{r}) \exp\left[-\gamma_{sp}(\mathbf{r}) \cos^2 \theta t\right] \quad (3)$$

After incorporating the distribution of emission dipoles and performing spatial averaging, we find that the predicted temporal emission decay curve and the emission rate distribution are in excellent agreement with experiments (Fig. 2e,f). Other than normalization, no fit parameters were used to obtain the simulated time-resolved decay curve and rate distribution. To probe the mechanisms and demonstrate control of emission rate enhancement, the gap thickness was tuned from $d = 5$ nm to 15 nm. Figure 3a presents the time-resolved emission from a single representative nanocube for each of four gap thicknesses. A non-exponential decay is observed for all samples, with a strong increase in emission rate with decreasing gap thickness. The simulated decay curves, obtained as described earlier, show excellent agreement with experiment. From the experimental emission rate distributions (Fig. 3b) we obtain three measures of emission rate enhancement as a function of gap thickness together with the simulated values (Fig. 3c). The maximum Purcell enhancement $\gamma_{sp}^{max}/\gamma_{sp}^{0}$ shows a strong dependence on gap thickness, increasing to ~2,000 for the $d = 5$ nm gap. These values are smaller than the simulated situation in Fig. 1e in which the dipoles are vertically oriented. The most likely rate enhancement $\gamma_{sp}^{*}/\gamma_{sp}^{0}$ shows similar trends to the maximum rate enhancement, but at lower values due to the non-optimal position of most emitters in the NPA.

The observed large emission rate enhancements are only desirable if the QE remains high. In general it is difficult to distinguish radiative enhancement from metal quenching because experimentally only the total emission rate is accessible directly. This ambiguity can be resolved by extracting the QE of the NPA from measurements of the time-integrated emission along with

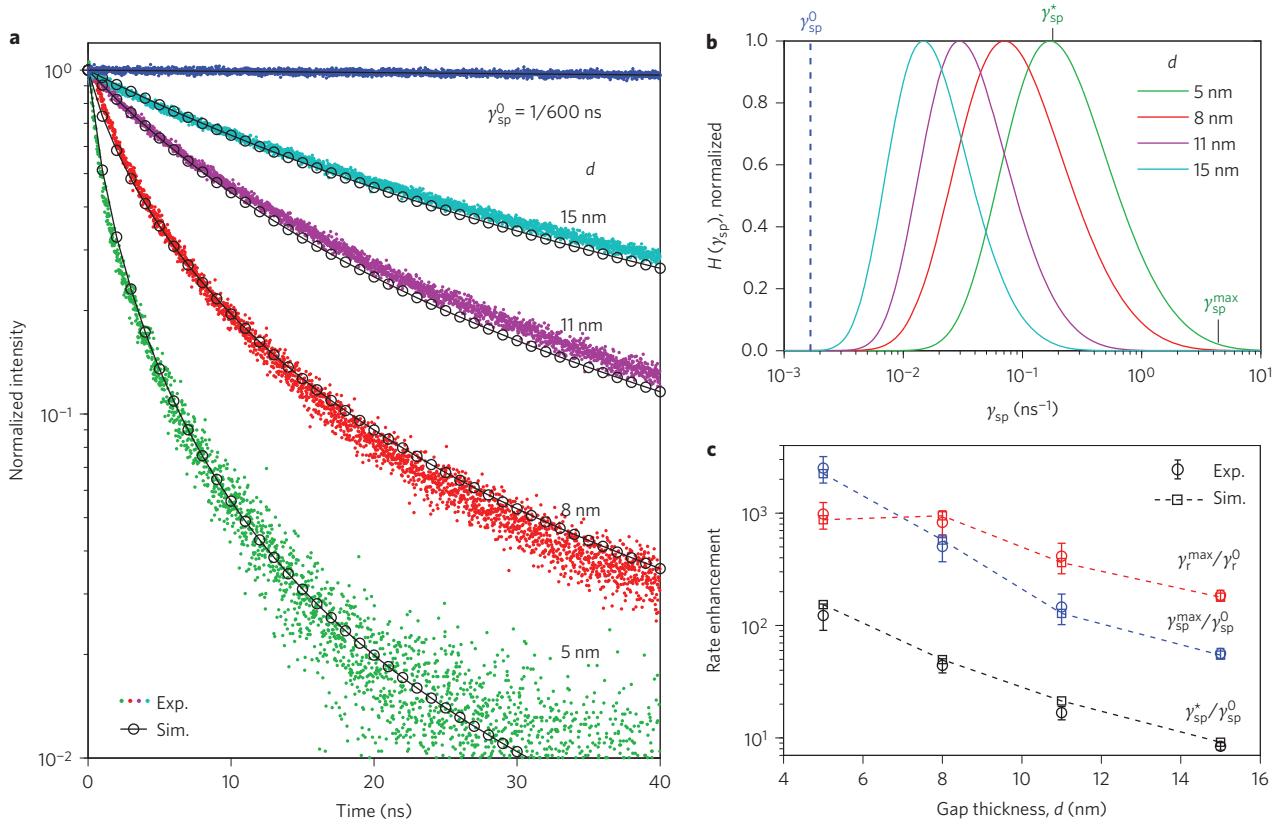

Figure 3 | Gap thickness dependence of spontaneous emission rates. a, Measured and simulated time-resolved Ru dye emission for four gap thicknesses *d*, with intensities normalized to $t = 0$. The decay is non-exponential for all gap thicknesses, which reflects the distribution of emission rates present for each nanocube. Each experimental curve is a measurement of a representative nanocube with the given gap thickness. **b**, Distribution of measured emission rates $H(\gamma_{sp})$ for each gap thickness as obtained from a stretched exponential fit followed by a Laplace transform. Rate distributions obtained from simulations are shown in Supplementary Fig. 3. The maximum spontaneous emission rate γ_{sp}^{max} is given by the slope of the time-resolved decay near $t = 0$. The most likely emission rate γ_{sp}^* is given by the mode of the rate distribution. **c**, Three measures of rate enhancement as a function of gap thickness, both from experiment and from simulations: (1) enhancement of the most likely emission rate $\gamma_{sp}^*/\gamma_{sp}^0$; (2) enhancement of the maximum spontaneous emission rate $\gamma_{sp}^{max}/\gamma_{sp}^0$ (Purcell enhancement), and (3) enhancement of the radiative rate given by $\gamma_r^{max}/\gamma_r^0 = \gamma_{sp}^{max}QE/\gamma_{sp}^0QE_0$, where QE is obtained from simulations (Fig. 4b).

simulations. To obtain the QE we first define the fluorescence enhancement factor (EF) relative to dipoles on glass:

$$EF = \frac{\eta}{\eta_0}\frac{\gamma_{ex}(\mathbf{r},\theta)}{\gamma_{ex}^0(\theta)}\frac{QE(\mathbf{r})}{QE_0} \quad (4)$$

where η is the emission collection efficiency and γ_{ex} is the excitation rate. Each of these values for the NPA is normalized by the same quantity calculated for equivalent dipoles on glass (Supplementary Figs 6 and 7). Figure 4a,b shows how the excitation rate enhancement and QE vary with gap thickness. The excitation rate enhancement is modest due to the non-resonant excitation and increases with decreasing gap size. The simulated QE remains high for a wide range of gap thicknesses greater than 6 nm, well above the intrinsic efficiency of the Ru dye, $QE_0 = 0.2$, taken as a typical QE of fluorescent dyes[33]. Furthermore, the QE at the position of highest emission rate enhancement, $\mathbf{r}_{max}$, is also high, pointing to the possibility of integrating single emitters with the NPA. Notably, due to the large emission rate enhancements, large enhancements in the radiative rate are possible even for embedded emitters with an intrinsically low QE.

Using the predicted collection efficiency of the NPA emission (Fig. 1d; 84%) and the emission from dipoles on glass (15%; Supplementary Fig. 7) the average EF, $\langle EF \rangle$, is obtained (Fig. 4c). To obtain experimental values for $\langle EF \rangle$, the ratio of emission from the NPA and the Ru-polymer films on glass was measured, normalized by the emissive area from each sample[29] (Supplementary Section 4). The experimental $\langle EF \rangle$, measured for approximately ten NPAs for each sample, shows excellent agreement with simulations without any fitting parameters. The variation in emission intensity between NPAs is probably due to the non-uniform distribution of Ru dye molecules in the polymer film, because a similar spot-to-spot variation was observed in the control sample emission. The accurate prediction of $\langle EF \rangle$ together with the accurate prediction of the emission decay rates (Fig. 3) provides direct validation that the radiative efficiency of the NPA is high and well described by the simulations in Fig. 4b. Having established the accuracy of the simulated QE of the system, we can determine the critical parameter of radiative rate enhancement. We find that, due to the high QE, the maximum radiative rate enhancement is $\gamma_r^{max}/\gamma_r^0 \approx 1{,}000$ for gaps $d \leq 8$ nm, which is higher than the $\gamma_{sp}^{max}/\gamma_{sp}^0$ for gaps where $d > 7$ nm (Fig. 4c). For gaps $d < 7$ nm, quenching of the dye emission by the metal becomes a significant loss mechanism.

The nanopatch antenna described here is a flexible platform for the enhancement of radiative properties with high efficiency and directionality. Although the present work intentionally utilizes emitters with slow intrinsic lifetimes, the rate enhancement of the NPA is independent of the intrinsic rates. Other short-lifetime and photostable emitters, such as quantum dots and crystal colour centres, can be integrated readily into the gap of the NPA. Furthermore, by optimal positioning and orientation of the

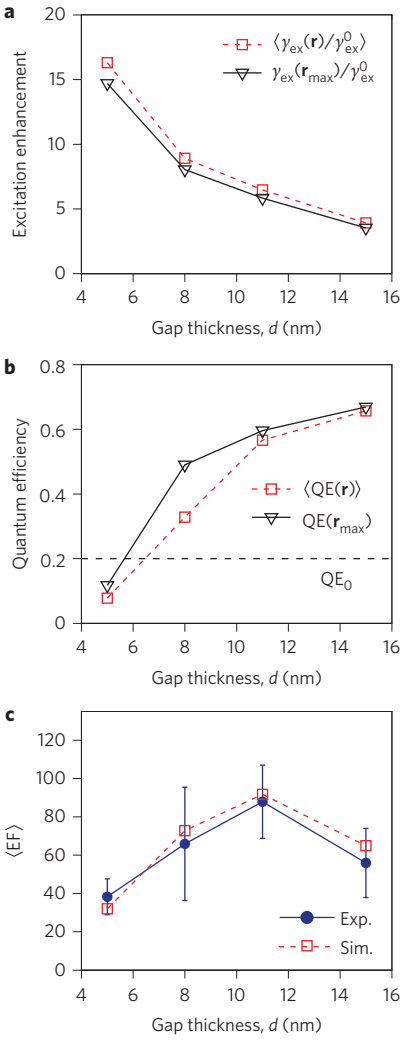

Figure 4 | Fluorescence intensity enhancement with high quantum efficiency. a, Simulated average excitation rate enhancement for dipoles in the nanogap relative to dipoles on glass. For each gap thickness, averaging is done over the lateral position of dipoles under the cube, over the vertical position in the gap and over the dipole orientation distribution. Also shown is excitation enhancement at the position of maximum emission rate enhancement, $\mathbf{r}_{max}$. **b**, Simulated average quantum efficiency (QE) as a function of gap thickness. The QE is high for a range of gap thicknesses and becomes smaller than the intrinsic quantum efficiency, QE_0, only for gaps d < 6 nm. Also shown is the QE at the position of maximum emission rate enhancement, $\mathbf{r}_{max}$. **c**, Measured and simulated average fluorescence enhancement factor per emitter ⟨EF⟩, as defined in equation (4). Measured and simulated ⟨EF⟩ are obtained entirely independently. The experimental error bars represent one standard deviation from a set of approximately ten measured NPAs for each gap thickness.

emitter dipoles via chemical[32] or other means, even larger rate enhancements are possible. For example, a vertically oriented dipole near the corners of the nanocube will experience a rate enhancement of 10,000, which for an emitter with a 10 ns intrinsic lifetime will produce terahertz-frequency operation. Furthermore, the NPA is a natural candidate for use as an efficient single-photon source or more generally as a fast nanoscale directional emitter.

Methods

Simulations. Finite-element simulations were used to calculate the scattering signature of the NPA and the electric field distributions induced at the nanogap both at excitation (535 nm) and resonant (650 nm) frequencies. The scattered-field formulation was employed, which uses the analytical solution for an incident plane wave in the absence of the nanocube as the background field. The Ru dye was modelled as a monochromatic point dipole emitting at $\lambda_{sp} = 650$ nm. The Green's function of the system, from which the local density of states, spontaneous decay rate and radiative QE can be derived[29], was evaluated by varying the position of the dipole emitter on a discrete 15×15 grid placed beneath the nanocube. The surface formed by this array was placed in different positions along the z axis inside the spacer layer to take into account, in our calculations, the entire volume of the nanogap. The radiative QE was obtained by calculating the total decay rate γ_{sp} of the dipole from Green's function (equations (1) and (2)) and calculating the non-radiative decay rate by integrating all metal losses over the volume of the NPA. The radiative QE is then given by $QE = 1 - \gamma_{nr}/\gamma_{sp}$ (see Supplementary Methods for more details).

Sample fabrication. The NPA samples were fabricated on 100-nm-thick template stripped gold substrates (Platypus Technologies). Immediately after separation from the template, the polymer spacer layer was grown on the gold substrate by immersion in a cationic solution of 3 mM poly(allylamine) hydrochloride (PAH) and 1 M NaCl for 5 min, followed by immersion in an anionic solution of 3 mM poly(styrenesulphonate) (PSS) and 1 M NaCl for 5 min. The samples were rinsed with a 1 M NaCl solution between successive layers. A 5 nm polymer layer was obtained from five polymer layers (terminating with PAH, as measured by spectroscopic ellipsometry), with other gap thicknesses shown in Supplementary Table 1. The polymer films were immersed for 5 min in a 1.8 mM aqueous solution of the Ru dye [(bis(2,2′-bipyridine)-4,4′-dicarboxybipyridine-ruthenium di(*N*-succinimidyl ester) bis(hexafluorophosphate)] (Sigma-Aldrich), followed by a thorough rinse in water. Control samples for the fluorescence enhancement measurements (Fig. 3c) were grown using the above procedure, but on a glass substrate. The correspondence between polymer film thickness on Au and glass substrates is shown in Supplementary Fig. 5. Nanocubes were not deposited on the glass control sample.

Silver nanocubes were chemically synthesized using previously described methods[28,34]. The resulting nanocubes had a corner radius of ~8 nm (determined by transmission electron microscopy, TEM) and a 3-nm-thick coating of polyvinylpyrrolidone (PVP) (Fig. 1c), which is a result of the synthesis procedure. Nanocubes were separated from other nanoparticles by centrifugation at 8,500 r.p.m., followed by resuspension in water and 1:100 dilution. A 25 µl drop of the nanocube solution was spread over the surface of the Ru-polymer film with a coverslip and incubated for 5 min. The negatively charged nanocubes electrostatically bound to the positively charged top polymer layer (PAH). After incubation, the non-adhered nanocubes were removed with a water rinse, and the sample was dried with nitrogen. The final nanocube surface density was ~0.01 μm^{-2}. Samples were measured within two days of fabrication to avoid silver oxidation, and were stored in a vacuum chamber when not being measured.

Optical measurements. Samples were measured using a custom-built fluorescence microscope (Supplementary Fig. 13). Individual NPAs were identified by dark-field imaging and spectroscopy to select only those NPAs with a resonance of $\lambda_{np} = 620$–650 nm. White light was coupled into the collar of a ×100, NA = 0.9 dark-field objective. Light scattered by the nanoparticles was collected by the same objective and imaged onto a charge-coupled device (CCD) camera. Individual NPAs were positioned in the centre of the field of view, and the scattered light from the particle was imaged onto a CCD spectrograph. A pinhole aperture at an intermediate image plane was used to select light only from the NPA of interest.

Once identified, time-resolved fluorescence emission from individual NPAs was measured in an epifluorescence configuration using time-correlated single-photon counting. The excitation source was a Ti:sapphire laser with an optical parametric oscillator, producing 200 fs pulses at $\lambda_{ex} = 535$ nm and a repetition rate of 80 MHz. The laser beam was passed through an electro-optic pulse picker to reduce the repetition rate to 20 MHz, followed by a 550 nm shortpass filter. The beam was then coupled into a single-mode optical fibre and collimated at the output, producing a Gaussian beam. The light was directed into the objective lens via a beamsplitter, filling the back aperture of the objective. The resulting focal spot was near diffraction-limited with a full-width at half-maximum of 350 nm. Emission from the NPA, which was positioned in the centre of the laser spot, was collected through the objective, passed through two 600 nm long-pass filters to remove the excitation laser, and imaged onto a single-photon counting avalanche photodiode (APD). The APD was connected to a timing module, which assembled a histogram of photon arrival times. The temporal resolution of the system was ~35 ps (Supplementary Fig. 1). All measurements were performed at an average power incident on the sample of 100 nW. Based on the dependence of emitted intensity as a function of excitation power, we conclude that measurements of all samples were carried out in the linear (unsaturated) regime (Supplementary Fig. 14).

Received 5 June 2014; accepted 2 September 2014; published online 12 October 2014

References

1. Claudon, J. *et al.* A highly efficient single-photon source based on a quantum dot in a photonic nanowire. *Nature Photon.* **4,** 174–177 (2010).
2. Kosako, T., Kadoya, Y. & Hofmann, H. Directional control of light by a nano-optical Yagi–Uda antenna. *Nature Photon.* **4,** 312–315 (2010).
3. Curto, A. G. *et al.* Multipolar radiation of quantum emitters with nanowire optical antennas. *Nature Commun.* **4,** 1750 (2013).
4. Hadden, J. P. *et al.* Strongly enhanced photon collection from diamond defect centers under microfabricated integrated solid immersion lenses. *Appl. Phys. Lett.* **97,** 241901 (2010).
5. Le Moal, E. *et al.* An electrically excited nanoscale light source with active angular control of the emitted light. *Nano Lett.* **13,** 4198–4205 (2013).
6. Noginov, M. A. *et al.* Demonstration of a spaser-based nanolaser. *Nature* **460,** 1110–1112 (2009).
7. Russell, K., Liu, T., Cui, S. & Hu, E. Large spontaneous emission enhancement in plasmonic nanocavities. *Nature Photon.* **6,** 459–462 (2012).
8. Schietinger, S., Barth, M., Aichele, T. & Benson, O. Plasmon-enhanced single photon emission from a nanoassembled metal–diamond hybrid structure at room temperature. *Nano Lett.* **9,** 1694–1698 (2009).
9. Oulton, R. F. *et al.* Plasmon lasers at deep subwavelength scale. *Nature* **461,** 629–632 (2009).
10. Eisaman, M. D., Fan, J., Migdall, A. & Polyakov, S. V. Invited review article: single-photon sources and detectors. *Rev. Sci. Instrum.* **82,** 071101 (2011).
11. Yablonovitch, E. Inhibited spontaneous emission in solid-state physics and electronics. *Phys. Rev. Lett.* **58,** 2059–2062 (1987).
12. Purcell, E. Spontaneous emission probabilities at radio frequencies. *Phys. Rev.* **69,** 681 (1946).
13. Gérard, J. *et al.* Enhanced spontaneous emission by quantum boxes in a monolithic optical microcavity. *Phys. Rev. Lett.* **81,** 1110–1113 (1998).
14. Englund, D. *et al.* Controlling the spontaneous emission rate of single quantum dots in a two-dimensional photonic crystal. *Phys. Rev. Lett.* **95,** 013904 (2005).
15. Bleuse, J. *et al.* Inhibition, enhancement, and control of spontaneous emission in photonic nanowires. *Phys. Rev. Lett.* **106,** 103601 (2011).
16. Vesseur, E. J. R., de Abajo, F. J. G. & Polman, A. Broadband Purcell enhancement in plasmonic ring cavities. *Phys. Rev. B* **82,** 165419 (2010).
17. Koenderink, A. F. On the use of Purcell factors for plasmon antennas. *Opt. Lett.* **35,** 4208–4210 (2010).
18. Anger, P., Bharadwaj, P. & Novotny, L. Enhancement and quenching of single-molecule fluorescence. *Phys. Rev. Lett.* **96,** 113002 (2006).
19. Filter, R., Słowik, K., Straubel, J., Lederer, F. & Rockstuhl, C. Nanoantennas for ultrabright single photon sources. *Opt. Lett.* **39,** 1246–1249 (2014).
20. Kinkhabwala, A. *et al.* Large single-molecule fluorescence enhancements produced by a bowtie nanoantenna. *Nature Photon.* **3,** 654–657 (2009).
21. Kollmann, H. *et al.* Toward plasmonics with nanometer precision: nonlinear optics of helium-ion milled gold nanoantennas. *Nano Lett.* **14,** 4778–4784 (2014).
22. Esteban, R., Teperik, T. V. & Greffet, J. J. Optical patch antennas for single photon emission using surface plasmon resonances. *Phys. Rev. Lett.* **104,** 026802 (2010).
23. Belacel, C. *et al.* Controlling spontaneous emission with plasmonic optical patch antennas. *Nano Lett.* **13,** 1516–1521 (2013).
24. Yi, M. *et al.* Plasmonic interaction between silver nano-cubes and a silver ground plane studied by surface-enhanced Raman scattering. *Plasmonics* **6,** 515–519 (2011).
25. Lassiter, J. B. *et al.* Plasmonic waveguide modes of film-coupled metallic nanocubes. *Nano Lett.* **13,** 5866–5872 (2013).
26. Ciracì, C. *et al.* Probing the ultimate limits of plasmonic enhancement. *Science* **337,** 1072–1074 (2012).
27. Yuan, C. *et al.* Modification of fluorescence properties in single colloidal quantum dots by coupling to plasmonic gap modes. *J. Phys. Chem. C* **117,** 12762–12768 (2013).
28. Moreau, A. *et al.* Controlled-reflectance surfaces with film-coupled colloidal nanoantennas. *Nature* **492,** 86–89 (2012).
29. Rose, A. *et al.* Control of radiative processes using tunable plasmonic nanopatch antennas. *Nano Lett.* **14,** 4797–4802 (2014).
30. Chen, Y., Munechika, K. & Ginger, D. S. Dependence of fluorescence intensity on the spectral overlap between fluorophores and plasmon resonant single silver nanoparticles. *Nano Lett.* **7,** 690–696 (2007).
31. Cang, H., Liu, Y., Wang, Y., Yin, X. & Zhang, X. Giant suppression of photobleaching for single molecule detection via the Purcell effect. *Nano Lett.* **13,** 5949–5953 (2013).
32. Lee, K. G. *et al.* A planar dielectric antenna for directional single-photon emission and near-unity collection efficiency. *Nature Photon.* **5,** 166–169 (2011).
33. Bakker, R. M. *et al.* Nanoantenna array-induced fluorescence enhancement and reduced lifetimes. *New J. Phys.* **10,** 125022 (2008).
34. Zhang, Q., Li, W., Wen, L.-P., Chen, J. & Xia, Y. Facile synthesis of Ag nanocubes of 30 to 70 nm in edge length with CF_3COOAg as a precursor. *Chem. Eur. J.* **16,** 10234–10239 (2010).

Acknowledgements

The authors thank A. Rose, R. Hill and A. Baron for discussions. This work was supported by the Lord Foundation of North Carolina and the Air Force Office of Scientific Research (contract no. FA9550-12-1-0491).

Author contributions

G.M.A. and M.H.M. conceived and designed the experiments. G.M.A. performed the experiments. C.A., G.M.A. and C.C. performed the simulations. G.M.A., C.A. and M.H.M. analysed the data. T.B.H. synthesized the Ag nanocubes. G.M.A., T.B.H., C.F. and J.H. fabricated and characterized the samples. G.M.A., C.A. and M.H.M. wrote the manuscript with input from all authors. M.H.M. and D.R.S. supervised the project.

Additional information

Supplementary information is available in the online version of the paper. Reprints and permissions information is available online at www.nature.com/reprints. Correspondence and requests for materials should be addressed to M.H.M.

Competing financial interests

The authors declare no competing financial interests.